CrossMark

# Interactions of the potent synthetic AT1 antagonist analog BV6 with membrane bilayers and mesoporous silicate matrices

G. Agelis [a], A. Resvani [a], D. Ntountaniotis [b], P. Chatzigeorgiou [b], C. Koukoulitsa [b], M.E. Androutsou [a], P. Plotas [a,c], J. Matsoukas [a,d], T. Mavromoustakos [b,*], T. Čendak [e], T. Ukmar Godec [e], G. Mali [e,f,**]

[a] Eldrug S.A., Patras Science Park, Stadiou, Platani, Rio Patras, 265 04, Greece
[b] Department of Chemistry, University of Athens, Athens, Greece
[c] Department of Medicine, University of Patras, Patras 265 00, Greece
[d] Department of Chemistry, University of Patras, Patras 26500, Greece
[e] Laboratory for Inorganic Chemistry and Technology, National Institute of Chemistry, Ljubljana, Slovenia
[f] EN-FIST Centre of Excellence, Ljubljana, Slovenia

## ARTICLE INFO

## ABSTRACT

The present work describes the drug:membrane interactions and a drug delivery system of the novel potent AT1 blocker BV6. This designed analog has most of the pharmacological segments of losartan and an additional biphenyltetrazole moiety resulting in increased lipophilicity. We found that BV6:membrane interactions lead to compact bilayers that may in part explain its higher in vitro activity compared to losartan since such environment may facilitate its approach to AT1 receptor. Its high docking score to AT1 receptor stems from more hydrophobic interactions compared to losartan. X-ray powder diffraction (XRPD) and thermogravimetric analysis (TGA) have shown that BV6 has a crystalline form that is not decomposed completely up to 600 °C. These properties are desirable for a drug molecule. BV6 can also be incorporated into a mesoporous silicate drug-delivery matrix SBA-15. The properties of the obtained drug-delivery system have been inspected by XRD, $^{13}$C CP/MAS, TGA and nitrogen sorption experiments.

© 2013 Published by Elsevier B.V.

## 1. Introduction

Coronary heart disease is one of the leading causes of death in the industrialized world. Hypertension is a risk factor for cardiovascular disease (CV) and is associated with an increased incidence of stroke and coronary heart disease. Other risk factors for CV include also high cholesterol, diabetes and obesity. Although there have been many advances in treatment over the past several decades, less than a quarter of all hypertensive patients have their blood pressure adequately controlled with available therapies. Early management of cardiovascular risk factors is fundamental in preventing the development of cardiovascular and renal disease [1,2].

The renin–angiotensin system (RAS) is known to play an important role in the regulation of blood pressure and electrolyte balance. Inhibitors of the RAS would be effective for the treatment of hypertension and congestive heart failure. Although angiotensin-converting enzyme (ACE) inhibitors are highly effective and their use has become well-established for the treatment of hypertension and congestive heart failure, they suffer from some side effects such as dry cough and angioedema caused by the nonspecific action of ACE. On the other hand, angiotensin II (AII) AT1 receptor blockers (ARBs) selectively interfere with the RAS at the AII receptor level and are expected to be more specific and effective agents than ACE inhibitors. The discovery of potent and orally active non peptide AII antagonists such as losartan and eprosartan has encouraged the development of a large number of similar compounds. Among them, candesartan cilexetil, valsartan, irbesartan, telmisartan and olmesartan medoxomil have been launched and were established as angiotensin receptor blockers (ARBs). Treatment with an ARB was demonstrated to reduce CV events and heart failure progression as well as to improve renal disease and prevent diabetes and this constitutes the importance of their development. Despite the plethora of treatment options for the management of hypertension, 55.9% of patients do not have their BP under adequate control. In addition, there is ambiguity concerning the appropriate choice of therapy for hypertensive patients who may present with coexisting conditions such as diabetes. Therefore, an agent with multifunctional purposes would offer an efficacious way of managing hypertension and related complications. Azilsartan medoxomil is a newer-generation ARB with potent antihypertensive effects. On 25 February 2011, the U.S. Food and Drug Administration (FDA) approved azilsartan medoxomil for the treatment of high blood pressure in adults [3–5].

* Corresponding author. Tel.: +30 210 7274475; fax: +30 210 7274761.
** Corresponding author. Tel +386 147 60412; fax: +386 147 60300.
    E-mail addresses: gregor.mali@ki.si (G. Mali), tmavrom@chem.uoa.gr (T. Mavromoustakos).

The molecular basis of their antihypertensive action has been interpreted by a two-step model. In the first step they are incorporated into the bilayers through the lipid–water interface and secondly laterally diffuse to reach the active site of the AT1 receptor in order to exert their biological activity [6].

BV6 (4-butyl-N,N -bis{[2 -(2H-tetrazol-5-yl)biphenyl-4-yl]methyl} imidazolium bromide) is a synthetic rationally designed molecule that exhibited higher activity than losartan (Fig. 1). This molecule comprises three well known pharmacophore segments identical to losartan, in particular the two biphenyltetrazole segments at the N-1 and N-3 of the imidazole ring and the butyl alkyl chain. However, it lacks the chlorine atom and hydroxymethyl group on the imidazole ring. Its higher activity can be postulated to be attributed to: (a) the way it interacts on the lipid bilayer as it is a more lipophilic entity; (b) the additional hydrophobic interactions that it can have at the active site of the receptor (Fig. 2) [7]. Estimated value of LogP for BV6 by ALOGPS 2.1 program was found to be 5.70 (for comparison reasons LogP of losartan was found to be 4.50) [8]. LogP values for all commercial sartans are given in Table 1. BV6 has the highest LogP value after telmisartan.

The cellular membranes are complex entities consisting of various kinds of proteins and lipids as well as cholesterol. Phosphatidylcholines (PCs) are the most abundant lipid species in sarcolemma cardiac membranes [9]. The most frequently found among them are PCs with oleic and linoleic chains, and further dipalmitoylphosphatidylcholine (DPPC). Experimentally, hydrated DPPC lipids are preferred because they spontaneously form multilamellar bilayers in which mesomorphic changes occur in a convenient temperature range between 25 and 50 °C. Their dynamic and thermotropic properties have been extensively explored [10–12] and their partition coefficient especially in the fluid state, resembles that of natural cardiac membranes [9]. Phosphatidyl choline bilayers at low temperatures occur in the gel phase ($L_{\beta}'$) and at higher temperatures in the liquid-crystalline phase ($L_{\alpha}$). The transition is accompanied by several structural changes in the lipid molecules as well as systematic alteration in the bilayer geometry, for example the trans:gauche isomerization taking place in the acyl conformation. The average number of gauche conformers indicates the effective fluidity, which depends not only on the temperature, but also on perturbation due to the presence of a drug molecule intercalating between the lipids.
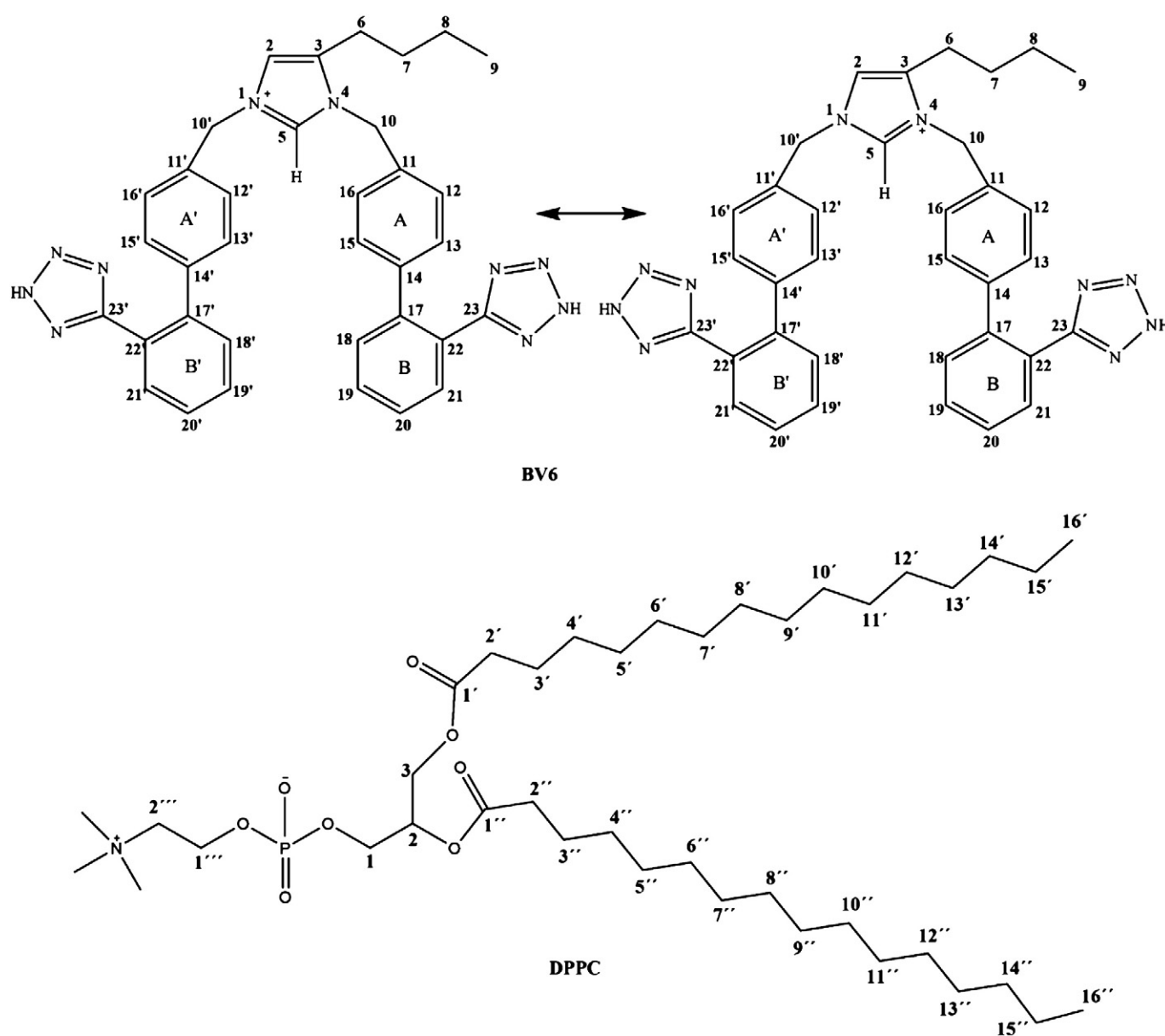


Fig. 1. Chemical structures of BV6 and $L_{\alpha}$-dipalmitoylphosphatidylcholine.
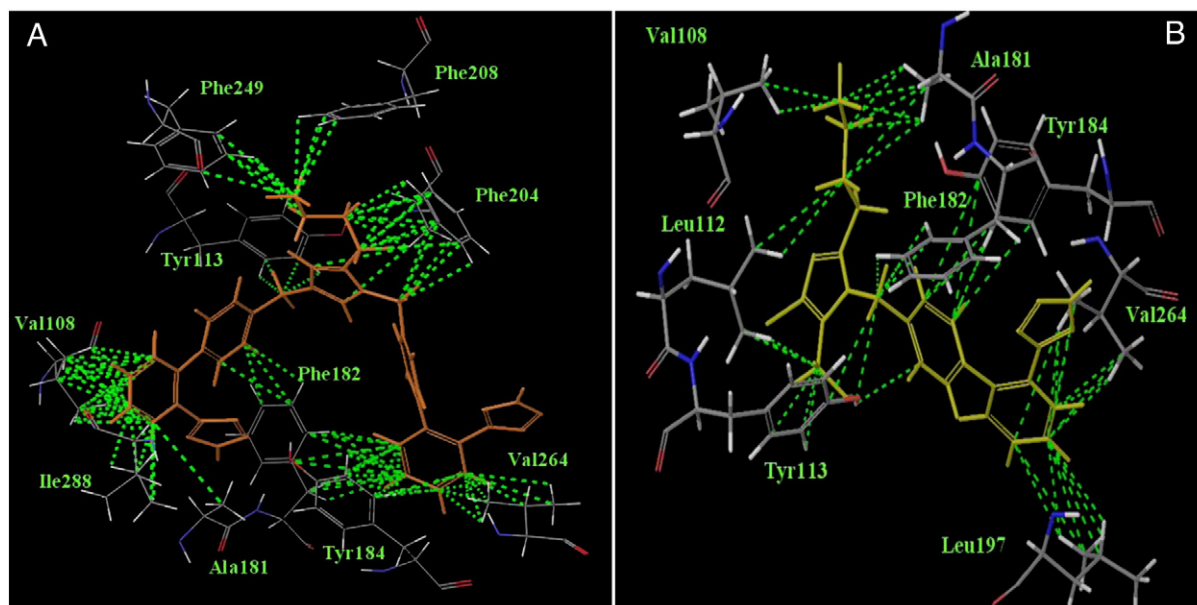
**Fig. 2.** Hydrophobic interactions of A. BV6 and B. losartan in the active site of AT1 receptor.

It is more and more evident that drugs affect the lipid core and form microdomains that modulate the activity of the vicinity of proteins and thus offer a new avenue in the membrane lipid therapy. A representative example is the drug:membrane interactions of the β2 agonists indacaterol and salmaterol which are characterized by different pharmacological properties. It was found that the synergy between the higher partitioning of indacaterol into the raft microdomains and the faster membrane permeation of indacaterol could explain the faster onset and longer duration of therapeutic effect of indacaterol. The higher fluidizing effect of salmeterol on membrane fluidity may contribute to its lower intrinsic efficacy compared to indacaterol [13]. Other studies postulated that active drugs do change the lateral pressure profile in bilayers and hence, can affect the behavior of membrane proteins [1–6,9–16]. As a consequence of this, every bioactive molecule has its special fingerprint when it interacts with membrane bilayers [17].

In this context, our laboratory has initiated research activity to study the effects of ARBs losartan, valsartan, olmesartan, CV-11974 and TCV-116 in membrane bilayers [18–21]. Thus, the significant amount of work performed on AT1 receptor blockers could also serve for comparative studies and further elaborate on the role of the drug in the cell membrane. In this study, the effects of the synthetic BV6 molecule intercalated in DPPC membranes were investigated and then were compared with the commercial ARB drugs.

An integrated approach using different complementary methodologies namely solid state $^{13}$C CP/MAS$^{13}$C MAS NMR spectroscopy,

HR-NMR spectroscopy, Differential Scanning Calorimetry (DSC), and Raman spectroscopy, have been applied. Briefly, DSC provides valuable information on the thermal modifications that are caused by the presence of drugs in the membrane [22]. Solid state NMR experiments offer useful information about the dynamic changes that drugs cause when they are incorporated in the lipid bilayers [22–25]. Typical observations are related with chemical shift or intensity changes of various key atoms which are partitioning in the membrane. Chemical shift changes are further associated with phase transition properties of the membrane bilayers. Moreover new peaks arise due to the presence of the drug. Raman experiments provide complementary structural information, for instance regarding the interdigitation effects of the molecules in lipid bilayers [26–28].

In the last part of the manuscript we discuss the solid (powder) form of BV6, and the drug-delivery system prepared from BV6 and the mesoporous silicate matrix SBA-15 [29]. The role of silicate-based drug-delivery systems in the transport of drugs through cell membranes has not been explored yet. Rather, the silicate-based drug-delivery systems were studied either to improve the availability of the drugs that are poorly soluble in physiological media or to enable controlled release of drugs in the body [30]. Since BV6 itself is well soluble in water-rich media, the main purpose of incorporating it into the mesoporous silicate matrix would be to gain control over the rate of the drug release (for example, to achieve prolonged release of the drug) or to gain control over the location of the drug release. On the internal and external surfaces, mesoporous silicates possess a significant amount of free silanol groups, which can be functionalized [31]. The attached functional groups can change physico-chemical properties of the surface and can therefore lead to specific interactions of the pharmaceutical system with the target environment or with the external stimuli. Some examples of functionalized mesoporous silicates used as matrices for site-specific or/and stimuli-responsive drug delivery include a polyamine-functionalized mesoporous silicate that releases drug only in neutral medium and not in the acidic one [32], SBA-15 functionalized with carboxylic groups that allow release of drugs only in acidic medium [33], and mesoporous silicate functionalized with superparamagnetic $Fe_3O_4$ nanoparticles, because of which the transport of drug-delivery particles within a body could be directed by external magnetic fields [34]. In this contribution we study only the possibility of the incorporation of BV6 into the mesoporous silicate SBA-15 matrix.

**Table 1**
LogP values of BV6 and AT1 antagonists calculated by ALOGPS 2.1 program [8].

| Compounds | LogP |
|---|---|
| BV6 | 5.70 |
| Losartan | 4.50 |
| Candesartan | 4.02 |
| Irbesartan | 4.51 |
| Valsartan | 3.68 |
| Olmesartan | 1.79 |
| Azilsartan | 4.50 |
| Telmisartan | 6.66 |
| Tasosartan | 3.07 |

## 2. Material and methods

### 2.1. Drug:membrane interaction system

#### 2.1.1. Differential Scanning Calorimetry

To prepare the samples for DSC experiments, appropriate amounts of DPPC and BV6 diluted in chloroform were mixed, dried under stream of argon and then stored under high vacuum overnight. Distilled and deionized water was added to the dried mixtures of DPPC–BV6 to produce a 50% (w/w) mixture/water preparation. The samples were transferred to stainless steel capsules obtained from Perkin-Elmer and sealed. Thermal scans were obtained on a Perkin-Elmer DSC-2 instrument (Norwalk, CT). All samples were scanned from 10 to 60 °C at least three times until identical thermal scans were obtained using a scanning rate of 2.5 °C/min. The temperature scale of the calorimeter was calibrated using indium ($T_m$ = 156.6 °C) and DPPC bilayers ($T_m$ = 41.2 °C).

The following diagnostic parameters were used for the study of drug to membrane interactions: $T_m$ (maximum position of the recorded heat capacity), $T_{onset}$ (the starting temperature of the phase transition) and $\Delta T_{m1/2}$ (the full width at half maximum of the phase transition), and the respective parameters concerning the pre-transition. An empty pan for the base line and a sample containing double distilled water were run for the temperature range of 10–60 °C as a reference for the background. This background was subtracted from each thermal scan of the samples. The area under the peak represents the enthalpy change during the transition ($\Delta H$). The mean values of $\Delta H$ of three identical scans were tabulated. The drug concentration used for the different experiments was $x$ = 0.20 (20 mol% BV6).

#### 2.1.2. Raman spectroscopy

Raman spectra were recorded with a Perkin-Elmer GX Fourier Transform spectrometer (Shelton, CT). A diode pumped Nd:YAG laser at 1064 nm (Norwalk, CT) was used as the excitation source. The scattered radiation was collected at an angle of 180° with respect to the incident beam. Spectra were recorded at a laser power of 400 mW on sample with a resolution of 2 cm$^{-1}$. To obtain a good signal-to-noise ratio, 2500 scans were coadded for each spectrum. The temperature was controlled using the high-temperature cell (CAL 3300, Ventacon Ltd., Winchester, UK). The intensity of a Raman band was observed over a period of 15 min. Analysis of the spectra was carried out using Spectrum Software Version No. 3.02.01 (Perkin-Elmer, Norwalk, CT). Raman spectra of the examined samples were obtained in the frequency region of 3500–400 cm$^{-1}$ and in the temperature range of 25 to 50 °C. The following ratios as a function of temperature were used for the study of drug to membrane interactions: $I_{1090}/I_{1130}$: This ratio allows the direct comparison of the bilayer disorder–order characteristics between bilayers preparations without or with drug incorporation [26,27]. $I_{2935}/I_{2880}$: This ratio measures the effects originating from changes both in interchain and intrachain order–disorder processes in the bilayer acyl chains. $I_{2850}/I_{2880}$: This ratio describes the main change occurring in the hydrocarbon-chain region of the lipids and corresponds to intermolecular interactions among aliphatic chains.

#### 2.1.3. High resolution liquid and solid state NMR

The high-resolution NMR spectra were recorded on a Varian 800 MHz spectrometer at 25 °C. Spectra were obtained with 2 mg of sample dissolved in 0.7 ml CD$_3$OD (Sigma Aldrich, St. Louis, MO). Default parameters installed in the library of the spectrometer were used. The $^1$H and $^{13}$C chemical shift assignments were obtained in a standard way using DQF-COSY, HSQC, and HMBC 2D experiments. Spectra were collected in the phase sensitive mode using the pulse sequences in the Varian library of pulse programs. Spectra allowed the unambiguous assignment of BV6.

The procedure to prepare the samples for $^{13}$C MAS and $^{13}$C CP/MAS spectroscopy was identical to that applied for DSC samples. Briefly, distilled and deionized water was added to the dried binary mixtures of DPPC/BV6 to produce a 50% (w/w) liposome dispersion. The samples

were transferred to 3.2 mm zirconia rotors. $^{13}$C NMR spectra were obtained at 150.80 MHz with a 600 MHz Varian spectrometer (Palo Alto, CA). The spinning rate used was 5 kHz. The experimental temperatures were 25 °C, 35 °C, and 45 °C for $^{13}$C CP/MAS experiments and 45 °C for the $^{13}$C MAS measurement.

### 2.2. Drug-delivery systems

BV6 was incorporated into the mesoporous silicate SBA-15 matrix. SBA-15 was synthesized according to Sayari et al. [35] using structure directing agent Pluronic P123 (PEG–PPG–PEG block copolymer, Aldrich) and tetraethyl orthosilicate (98% TEOS, Aldrich) as a silica source. Drug-loading procedure started by dissolving 70 mg of BV6 in 1 g of dimethyl sulfoxide (DMSO). The solution was added dropwise to fine layer of calcined SBA-15, allowing the powder to soak up the added drops. The obtained sample was then dried using a two step drying procedure combining drying at 313 K for 24 h in a ventilation dryer followed by drying at 313 K for 24 h in a vacuum dryer. The obtained composite was denoted as SBA-15/BV6.

#### 2.2.1. X-ray powder diffraction (XRPD)

XRPD patterns of solid samples were recorded on a PANalytical X'Pert PRO high-resolution diffractometer using CuKα1 radiation (1.5406 Å) in the 2θ range between 5° and 35°, taking 100 s for a step of 0.033°. For the SBA-15/BV6 composite XRPD pattern was recorded also in the 2θ range between 0.5° and 5°.

#### 2.2.2. Thermogravimetric analysis (TG)

Thermogravimetric analyses (TG) were carried out between 298 K and 873 K with a heating rate of 20 K/min using Mettler Toledo (Schwerzenbach, Switzerland) thermo-gravimetric analyzer model TGA/DSC 1 under a constant gas flow rate (oxygen, 50 mL/min). The initial sample masses ranged between 3 and 5 mg.

#### 2.2.3. Nitrogen adsorption–desorption measurement

Adsorption and desorption isotherms of nitrogen were measured on a Micromeritics ASAP 2020 volumetric adsorption analyzer at 77 K. Before the sorption analysis, SBA-15 and SBA-15/BV6 samples were outgassed under vacuum for 4 h at 373 K. The BET specific surface areas ($S_{BET}$) were estimated using adsorption data in the relative pressure range between 0.05 and 0.22 for SBA-15 and between 0.03 and 0.24 for SBA-15/BV6. The total pore volumes ($V_t$) for the empty matrix and for the drug-delivery system were estimated from the amounts of nitrogen adsorbed at relative pressures of 0.953 and 0.943, respectively, converting them to the volumes of liquid nitrogen at 77 K. The microporosity ($V_{mi}$) was determined by the t-plot method. The pore size distribution was obtained by analyzing the adsorption data of the sorption isotherm using the DFT approach.

#### 2.2.4. $^{13}$C CP/MAS NMR spectroscopy

$^{13}$C CP/MAS NMR spectra were recorded on a 600 MHz Varian NMR System equipped with a 3.2 mm Varian MAS probehead. Larmor frequency for $^{13}$C nuclei was 150.812 MHz, relaxation delay was 5 s, CP contact time was 5 ms, and sample rotation frequency was 16 kHz. Chemical shift was reported relative to the signal of $^{13}$C nuclei in tetramethylsilane.

## 3. Results

### 3.1. Drug:membrane interactions

#### 3.1.1. Differential Scanning Calorimetry

In previous studies we used Differential Scanning Calorimetry to detect the thermal changes caused by AT1 receptor blockers when they were incorporated in the lipid bilayers. We found out that $x$ = 0.20 was the most critical to detect differential effects. For this reason, we have chosen this concentration as a representative for comparison
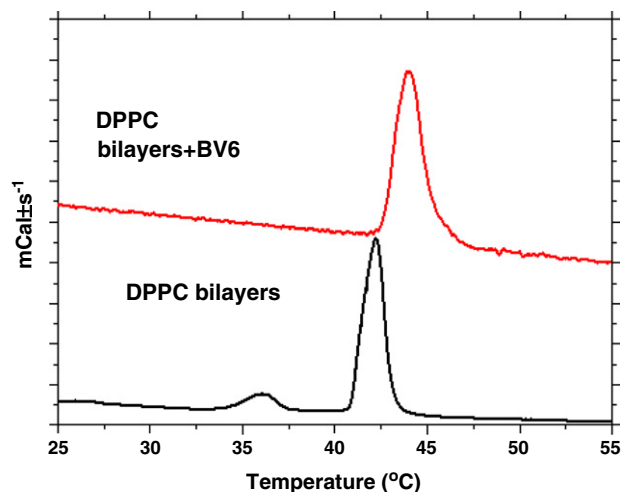
**Fig. 3.** Differential Scanning Calorimetry scans of DPPC bilayers alone (bottom) and DPPC bilayers containing $x = 0.20$ of BV6 (top).

with other AT1 receptor blockers already studied. The DSC results shown in Fig. 3 revealed that BV6 causes enhancing of the bilayer packing shifting the $T_m$ from 42.2 °C to the higher value of 43.81 °C (the corresponding $T_{onset}$ for the bilayer with and without BV6 were 42.49 °C and 40.91 °C) and caused increase in $\Delta H$ (7.98 kcal/mol versus 6.95 kcal/mol observed for the lipid bilayers alone). BV6 caused abolishment of the pre-transition temperature.

### 3.1.2. Raman spectroscopy

The methylene C−H stretching mode region 2800–3100 cm$^{-1}$ provides the most intense bands in the Raman spectrum of lipid samples and is commonly used to monitor changes in the lateral packing properties and mobility of the lipid chain in both gel and liquid crystalline bilayer systems. In particular, the intensity ratio $I_{2850}/I_{2880}$ provides an order parameter of the bilayer core. Indeed, this ratio indicates that bilayers with incorporated BV6 are more ordered than pure DPPC bilayers in accordance with DSC data (see Fig. 4A).

The C−C stretching mode region in the 1050–1150 cm$^{-1}$ spectral interval reflects directly intramolecular *trans:gauche* conformational changes within the hydrocarbon chain region of the lipid matrix. More importantly, the temperature profiles of the peak height intensity ratio $I_{1090/1130}$ allows the direct comparison of the bilayer disorder–order characteristics between bilayer preparations without or with BV6. BV6 induces lowering of *gauche:trans* ratio (see Fig. 4B).

The peak height intensity $I_{2935}/I_{2880}$ ratio constitutes a sensitive probe to monitor the lipid phase transitions despite the fact that the C−H stretching mode region consists of many superimposed vibrational transitions. Fig. 4C shows changes in $I_{2935}/I_{2880}$ peak height intensity ratio caused by BV6, when incorporated in DPPC bilayers. DPPC bilayers alone and those containing BV6 resemble the corresponding ones of the ratio $I_{1090}/I_{1130}$.

Various other bands are examined (not shown). For example the band at 714 cm$^{-1}$ is shifted to 717 cm$^{-1}$ showing strong interaction of BV6 with polar region. Bands corresponding to −CH$_3$ or −CH$_2$ were not significantly affected. The bands at 1600 cm$^{-1}$ and 1620 cm$^{-1}$ which correspond to the asymmetric and symmetric stretch vibrations of the C═C bonds clearly confirm the incorporation of BV6 in the lipid bilayers.

### 3.1.3. $^{13}C$ MAS and CP/MAS NMR spectroscopy

We have applied high-resolution NMR spectroscopy using magic angle spinning without or with cross polarization to obtain detailed local information on the incorporation of BV6 in the DPPC bilayers.
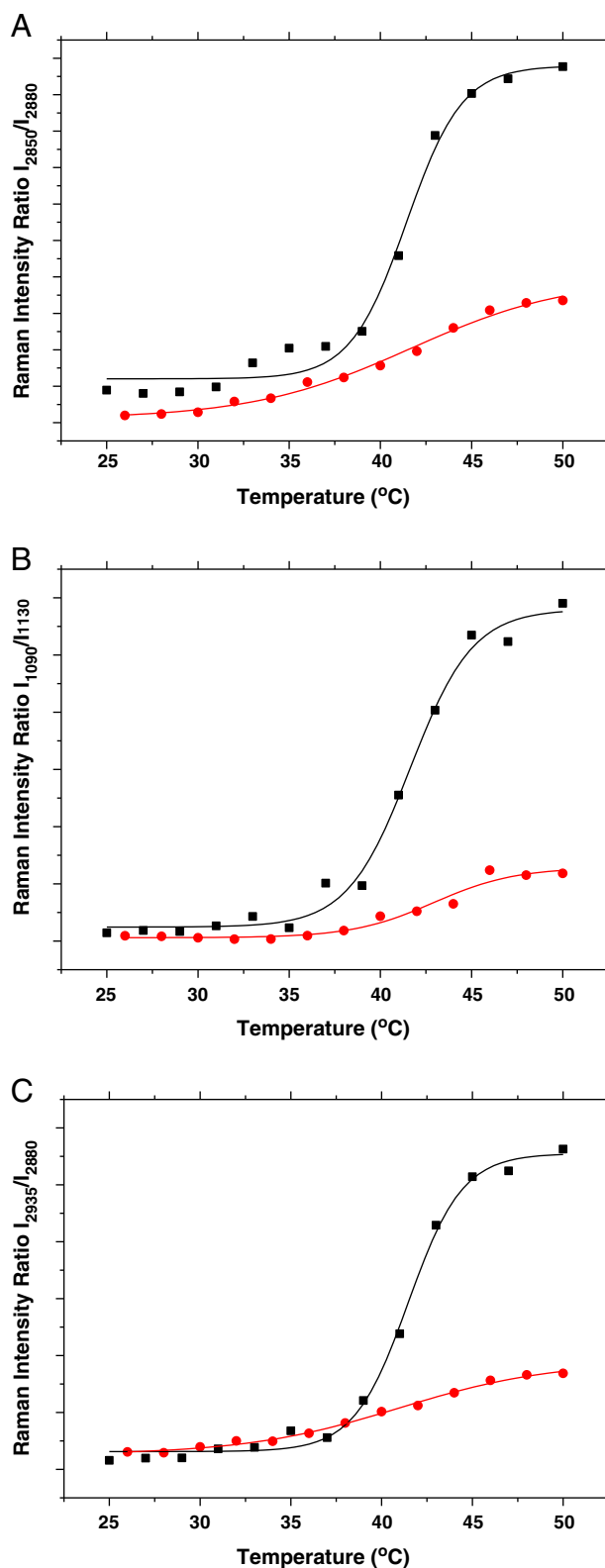


**Fig. 4.** Raman intensity ratios vs. temperature plots for pure DPPC (squares) and DPPC containing x = 0.20 of BV6 (circles).

Each spectrum was divided into three regions, namely concerning the carbon atoms in the (i) hydrophobic region (10–40 ppm), those in (ii) head-group, glycerol backbone regions and region containing carbons between aromatic segments (55–80 ppm) and (iii) aromatic and esterified carbonyls (125–180 ppm) (see Fig. 5).
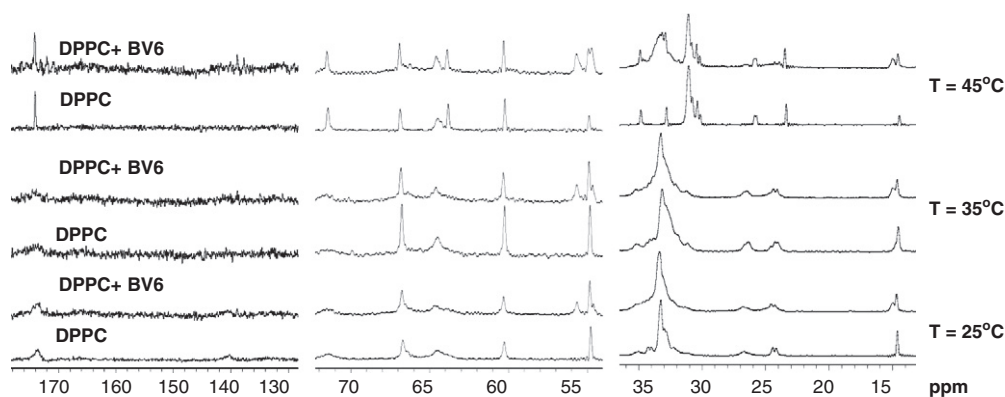
**Fig. 5.** $^{13}$C NMR CP/MAS spectra of DPPC bilayers with and without BV6 at three temperatures covering all the mesomorphic states of the lipid bilayers.

*3.1.3.1. Hydrophobic region.* The chemical shift decreases (upfield effect), when DPPC bilayers undergo the transition from the lamellar gel phase $L_{\beta}'$ (25 °C) towards the ripple phase $P_{\beta}'$ (35 °C) and lamellar liquid crystalline phase $L_{\alpha}$ (45 °C) (see Table 2 and Fig. 6). This is due to the strong *trans:gauche* isomerization effects observed especially in the turnover to the $L_{\alpha}$ phase. For example, we detected an upfield change between 0.2 and 2.2 ppm for $(CH_2)'_{10}$, C-14′, C-15′ and C-16′ signifying the same trend and different extent of upfield effect of the carbons that constitute the hydrophobic region. Upfield effect (0.1–2.3 ppm) was also observed in DPPC/BV6 bilayers. Generally, at the same temperature the values for samples containing BV6 were slightly higher.

A peak at ca 15 ppm was observed which is attributed to the terminal carbon of the methyl group (C9) of the butyl alkyl chain of BV6 as was elucidated using a combination of 1D and 2D NMR spectra (not shown). Approximately at 25 ppm an eminent additional peak is attributed to C8 of the alkyl chain. Several peaks of small intensity

have been observed in the aromatic region. To examine the effect of cross polarization we have run the same experiments at 45 °C using MAS without applying cross polarization. Indeed all additional peaks were also observed in MAS experiment (Fig. 6).

*3.1.3.2. Head-group, glycerol backbone regions and region containing carbons between aromatic segments.* Smaller chemical shift changes were observed for the two preparations used in our experiments indicating that head-group conformational changes from gel to liquid crystalline phase are less pronounced compared to that observed in the hydrophobic region (Table 2). Specifically, a downfield shift (<0.2 ppm) was observed during the phase transition from the gel to liquid crystalline state for the two preparations for the carbons of the head-group indicating, as is already mentioned, its conformational stability in this bilayer region. Steadily, as in the hydrophobic region the preparation containing BV6 had a slighter higher chemical shift than the pure DPPC bilayers.

**Table 2**
Observed chemical shifts for DPPC carbons in $^{13}$C MAS and $^{13}$C CP/MAS experiments.

**$^{13}$C MAS**

| T (°C) | Sample | C-X C-1 | C-2 | C-3 | C-1′, C-1″ | C-2′, C-2″ | C-3′, C-3″ | $(CH_2)'_{10}$, $(CH_2)''_{10}$ | C-14′, C-14″ | C-15′, C-15″ | C-16′, C16″ | $N(CH_3)_3$ | C-2‴ | C-1‴ |
|---|---|---|---|---|---|---|---|---|---|---|---|---|---|---|
| 45 | DPPC | 63.80 | 71.41 | 64.41 | 174.02 | 34.81 | 25.86 | 31.10 | 32.83 | 23.41 | 14.49 | 54.89 | 66.82 | 60.21 |
|  | DPPC/BV6 | 63.90 | 71.53 | 64.54 | 174.15 | 34.86 | 25.79 | 31.09 (+3 shoulders) | 32.91 33.12 | 23.48 | 14.58 | 54.95 | 66.91 | 60.32 |

**$^{13}$C /MAS**

| T (°C) | Sample | C-1 | C-2 | C-3 | C-1′, C-1″ | C-2′, C-2″ | C-3′, C-3″ | $(CH_2)'_{10}$, $(CH_2)''_{10}$ | C-14′, C-14″ | C-15′, C-15″ | C-16′, C16″ | $N(CH_3)_3$ | C-2‴ | C-1‴ |
|---|---|---|---|---|---|---|---|---|---|---|---|---|---|---|
| 25 | DPPC | – | 71.22 | 64.38 | 172−175 | 34.98 | 26.72 | 33.25 | 34.22 | 24.45 | 14.65 | 54.76 | 66.63 | 60.22 |
|  | DPPC/BV6 | – | 71.54 | 64.71 | 173.95−175.55 | – | 26.77 | 33.35 | – | 24.26 +24.55 | 14.67 | 54.86 | 66.78 | 60.35 |
| 35 | DPPC | – | 71.14 | 64.38 | 172−175 | 35.10 | 26.37 | 33.11 | – | 24.25 | 14.60 | 54.79 | 66.69 | 60.20 |
|  | DPPC/BV6 | – | 71.55 | 64.61 | 173.83−174.48 | 35.19 | 26.48 | 33.25 | – | 24.10 +24.39 | 14.65 +14.99 | 54.91 | 66.83 | 60.34 |
| 45 | DPPC | 63.77 | 71.37 | 64.49 | 174.03 | 34.81 | 25.85 | 31.06 | 32.79 | 23.39 | 14.49 | 54.86 | 66.81 | 60.19 |
|  | DPPC/BV6 | – | 71.60 | 64.58 | 174.27 | – | 25.85 | 31.08+33.27 | – | 23.58 | 14.80 | 54.90 | 66.91 | 60.35 |
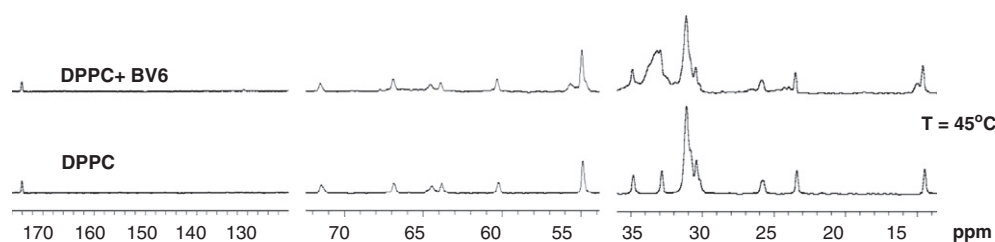


**Fig. 6.** $^{13}$C NMR MAS spectra of DPPC bilayers with and without BV6 at 45 °C.

An additional peak close to 55 ppm is observed which corresponds to C10′ methylene group of BV6. This was also observed in MAS experiments.

### 3.1.4. Aromatic and carbonyl regions

Only at 45 °C the aromatic region of BV6 is eminent but still contains low intensity peaks. To test if this is due to inefficient cross polarization we observed the corresponding MAS spectra. Clearly, in the MAS spectra these peaks are still of low intensity signifying the fact that their low intensity is attributed to rigidity of the bilayers when BV6 is incorporated rather than inefficient cross polarization.

The resolution of C-1′ in the carbonyl region for the two preparations was not satisfactory to follow the chemical shift changes during the phase transition. However, from the shape of the peaks it can be realized that DPPC bilayers containing BV6 are more rigid compared to the pure DPPC bilayers.

### 3.2. Analysis of the solid form and of the drug-delivery system

X-ray diffraction pattern of the powdered BV6 (Fig. 7A) exhibits sharp diffraction peaks and shows that the neutral substance is a crystalline material. The $^{13}$C CP/MAS NMR spectrum (Fig. 7B) also exhibits relatively narrow lines, which, however, overlap substantially so that the contributions from the various carbon sites cannot be easily resolved. (A tentative assignment of the resonances is presented in Fig. 7B.) Carbon signals resonating at about 160 ppm can be assigned to carbon atoms of the tetrazole rings of BV6. It seems that the packing of BV6 molecules within the crystals is such that either the two carbon sites within the two tetrazole rings of the same molecule experience slightly different environments or that two (crystallographically inequivalent) BV6 molecules comprise the crystallographic asymmetric unit.

The diffraction pattern of the drug-delivery system obtained after the incorporation of BV6 into the mesopores of SBA-15 exhibits diffraction peaks only in the range between 0.5° and 2°. These peaks are characteristic for the ordered hexagonal arrangement of the mesopores of the silicate matrix [29]. Obviously, the BV6 molecules are too large and the pores of SBA-15 with the diameter of approximately 11 nm are too narrow that (sufficiently large) crystallites, which would give rise to narrow diffraction maxima at higher diffraction angles, could be formed. As opposed to the diffraction maxima, the signals within the $^{13}$C CP/MAS NMR spectrum of BV6 within the delivery system are still clearly visible and only slightly broader from the signals of the bulk crystalline substance. A new narrow signal at about 40 ppm belongs to the trace of solvent. Apparently the drying procedure leaves traces of DMSO molecules within the pores.

The spectra of the powdered BV6 and the BV6 incorporated within SBA-15 both exhibit two resolved signals of the tetrazole carbon nuclei. Since the packing of the neutral BV6 molecules within the pores of SBA-15 is most probably different from the packing of these molecules within the pure crystals, the two slightly different environments for carbon nuclei within the two tetrazole rings must stem from the asymmetry of a BV6 molecule alone and do not belong to carbon nuclei from two separate BV6 molecules.

The crystalline BV6 and the drug-delivery system based on the substance were submitted also to thermogravimetric analysis (Fig. 8). Somewhat surprisingly, in the temperature range between 25 °C and 600 °C BV6 was not entirely decomposed. This is most probably due to the fact that BV6 is actually a salt and salts typically exhibit very high melting points. For the drug-delivery system the loss of mass within the above mentioned temperature interval was even smaller, which is understandable, knowing that the silicate mesoporous matrix is completely stable up to 600 °C [29] and that the observed mass loss was only due to the (partial) removal of the drug from the pores of the drug-delivery system. If the reduction of the mass of drug within the delivery system is comparable to the reduction of the mass of drug in the bulk form, then the initial mass fraction $m(BV6)/m(SBA-15/BV6)$
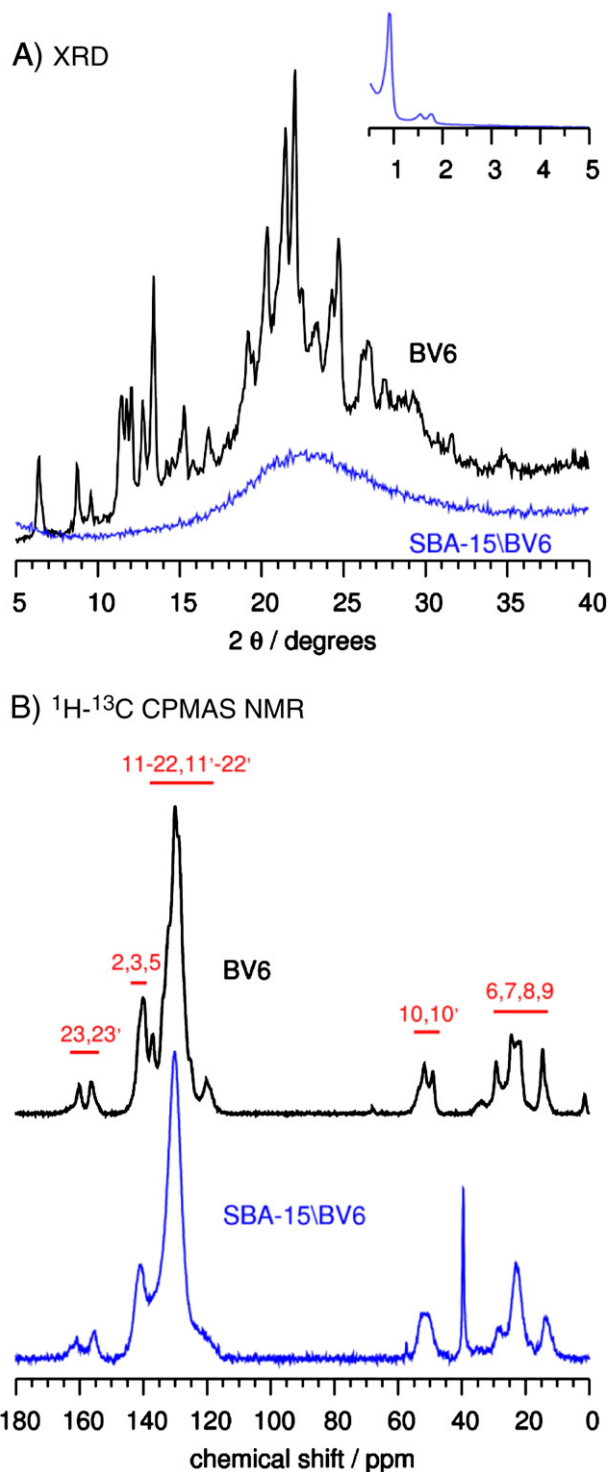


**Fig. 7.** XRPD patterns (A) and $^{13}$C CP/MAS NMR spectra (B) of the bulk substance BV6 and of the drug-delivery system SBA-15/BV6. Plot (B) contains tentative assignment of $^{13}$C CP/MAS NMR signals to carbon atoms within BV6. The numbers above the horizontal lines correspond to carbon-atom labels as used in Fig. 1.

can be estimated to be approximately 0.55. This fraction is quite high and exceeds the one that was observed for the drug-delivery systems in which indomethacin was incorporated into SBA-15 [36,37]. If, however, up to 600 °C all the drug is expelled from the pores of the matrix, then the initial mass fraction $m(BV6)/m(SBA-15/BV6)$ can be estimated to be approximately 0.35.
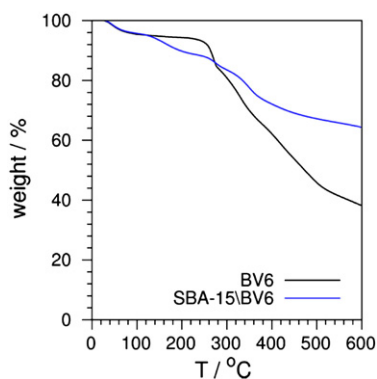
**Fig. 8.** TG profiles of the bulk BV6 and of the drug-delivery system SBA-15/BV6.

**Table 3**
Specific surface areas and pore volumes of SBA-15 and SBA-15/BV6 samples.

| Sample | $S_{BET}$ (m$^2$/g) | $V_t$ (cm$^3$/g) | $V_{mi}$ (cm$^3$/g) |
| --- | --- | --- | --- |
| SBA-15 | 662 | 0.90 | 0.07 |
| SBA-15/BV6 | 197 | 0.33 | 0.02 |

packing of lipid bilayers when BV6 is intercalated may explain its suitable fit in the core of the lipid bilayers and easy approach at the AT1 active site resulting in high in vitro activity.

*4.2. Raman spectroscopy*

The decrease of the mobility and *gauche:trans* ratio observed in the Raman spectroscopy is in agreement with DSC results which show that BV6 strengthens the packing of the lipid bilayers. Also in the ratio of $I_{2935}/I_{2880}$ a shift was observed in higher temperatures in accordance with DSC results. The strong interactions observed for BV6 with head-group were in accordance with DSC results where an abolishment of pre-transition was observed. The direct incorporation of BV6 in lipid core was observed by detecting C=C vibration stretches in the region of 1600–1620 cm$^{-1}$. This is again in harmony with DSC results which showed a differential thermal scan profile of the bilayer containing BV6 in comparison with DPPC bilayers without the drug. The ratio $I_{2850}/I_{2880}$ is considered also to be diagnostic for interdigitation effects. As with most of the commercial AT1 antagonists, BV6 appears to cause interdigitation effects in accordance with DSC data which showed increase of $\Delta H$ and $T_m$.

To gain some additional insight into the prepared drug delivery system, finally, SBA-15/BV6 and the parent SBA-15 material were subjected to the nitrogen sorption analysis. This analysis is an important approach for the inspection of the porosity of the materials. The measured adsorption–desorption isotherms and the derived pore-size distribution profiles are presented in Fig. 9 and the quantitative data on the specific surface area and pore volume of the two materials are listed in Table 3. In the figure we can see that both nitrogen adsorption–desorption isotherms are of type IV sorption isotherms according to the IUPAC classification and exhibit well-defined H1 hysteresis loops, which are typical for SBA-15 silicates. The presence of H1 hysteresis type confirms that the parent material and the drug-delivery system have open-ended cylindrical mesopores. One can also see that after the impregnation of the mesoporous silicate matrix with the BV6 drug, the pore volume and the specific surface area were reduced drastically — to approximately one third of the initial value. This is an indication that indeed a substantial amount of the drug was incorporated into the pores of SBA-15.

## 4. Discussion

*4.1. DSC*

The incorporated BV6 in lipid bilayers exerts similarities and differences in thermal effects when these are compared with those exerted by the commercial AT1 receptor blockers. The similarities are expressed in: (a) abolishment of the pre-transition; (b) increase of the breadth of the phase transition and (c) increase of $\Delta H$. However, BV6 is the only active AT1 antagonist studied so far that causes also increase in $T_m$ probably due to the fact that augments hydrophobic interactions when it is embedded in the lipid bilayers. This favored

*4.3. Solid state $^{13}C$ CP/MAS and $^{13}C$ MAS*

In our previous studies we have observed that intensities in the aromatic region depend on the rigidity of the system. When prototype AT1 receptor blocker was incorporated in DPPC bilayers we were able to structurally elucidate all the peaks attributed to the aromatic region [6].

This was not observed, however, in the case of DPPC bilayers containing olmesartan where the aromatic region is more extended [19]. In the case of BV6, the aromatic region is even more extended and this leads to even more rigid system. Makriyannis et al observed an identical relationship between GPCR cannabinoid agonists that act on the head-group vicinity as it is recently reported by using solid state $^2H$ NMR spectroscopy. More specifically, the more rigid $\Delta^8$-tetrahydrocannabinol compared with CP-55940 (synthesized by Pfizer) and WIN-55212-2 (discovered by the Sterling Winthrop research team) increased to a greater degree the order parameter of the bilayer core [38].
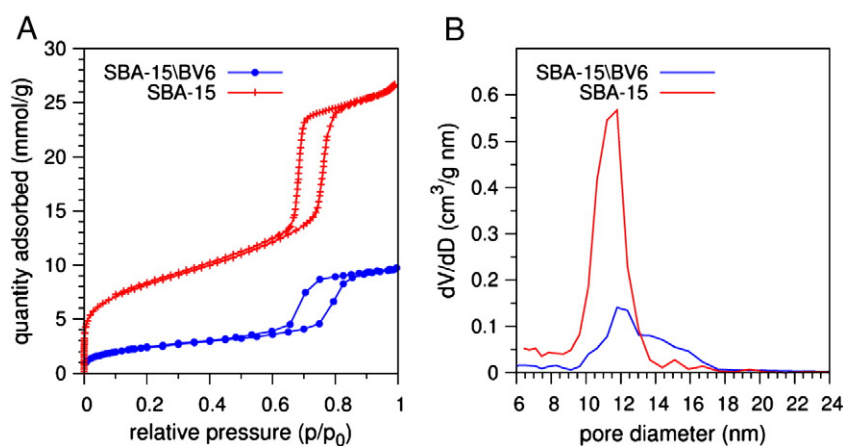


**Fig. 9.** Nitrogen sorption isotherms (A) and pore size distributions (B) of SBA-15 and SBA-15/BV6.

## 4.4. Solid form and drug-delivery system

XRD and NMR analyses showed that the solid form of BV6 is crystalline. The substance probably shows crystalline structure because it is a salt, in which the positive charge on the imidazole ring is neutralized by the $Br^-$ anion. Of course, salts are usually substances that crystallize easily.

BV6 could be incorporated into the mesopores of the mesoporous silicate matrix SBA-15 with a high filling fraction. The incorporated substance resembles amorphous materials. Taking into account that the chemical shifts for the bulk substance and the substance embedded within the mesopores are almost the same, BV6 molecules most probably interact with the silicate walls very weakly. Of course, the interaction, which eventually influences the drug-release rate, could be altered by the functionalization of the mesoporous silicate matrix.

## 5. Conclusions

We have studied the drug:membrane interactions and drug-delivery system of a novel synthetic AT1 antagonist BV6 that possesses higher in vitro activity than prototype drug in sartan class losartan. Although it has almost all pharmacophoric segments of losartan, the novel analog BV6 is bulkier and more lipophilic. Its high lipophilicity in conjunction with its amphiphilic properties constitutes the driving force for its intercalation in the lipid bilayers and increase of their packing abilities. These properties are observed also with commercial AT1 antagonists but to a lesser extent. Since BV6 has these desirable properties in the lipid bilayers that may explain in part its diffusion ability to the AT1 receptor and its favorable binding, we found it interesting to investigate its physico-chemical and delivery properties in SBA-15 system. Its crystalline properties and especially high stability in decomposition are highly desirable properties for a drug. Its size and shape allow its packing into the delivery SBA-15 system with a relatively high efficiency.

## Acknowledgement

## References

[1] P. Verdecchia, F. Angeli, S. Repaci, G. Mazzotta, G. Gentile, G. Reboldi, Comparative assessment of angiotensin receptor blockers in different clinical settings, Vasc. Health Risk Manag. 5 (2009) 939–948.

[2] J.M. Neutel, Choosing among renin–angiotensin system blockers for the management of hypertension from pharmacology to clinical efficacy, Curr. Med. Res. Opin. 26 (2010) 213–222.

[3] P. Naik, P. Murumkar, R. Giridhar, M.R. Yadav, Angiotensin II receptor type 1 (AT1) selective nonpeptidic antagonists—a perspective, Bioorg. Med. Chem. 18 (2010) 8418–8456.

[4] W. White, M. Weber, D. Sica, G. Bakris, A. Perez, C. Cao, S. Kupfer, Effects of the angiotensin receptor blocker azilsartan medoxomil versus olmesartan and valsartan on ambulatory and clinic blood pressure in patients with stages 1 and 2 hypertension, Hypertension 57 (2011) 413–420.

[5] M. De Gasparo, K.J. Catt, T. Inagami, J.W. Wright, Th. Unger, International Union of Pharmacology. XXIII. The angiotensin II receptors, Pharmacol. Rev. 52 (2000) 415–472.

[6] P. Zoumpoulakis, I. Daliani, M. Zervou, I. Kyrikou, E. Siapi, G. Lamprinidis, E. Mikros, T. Mavromoustakos, Losartan's molecular basis of interaction with membranes and AT1 receptor, Chem. Phys. Lipids 125 (2003) 13–25.

[7] G. Aggelis, A. Resvani, C. Koukoulitsa, T. Tumonva, J. Slaninova, D. Kalavrizioti, K. Spyridaki, A. Afantitis, G. Melagraki, A. Siafaka, E. Gkini, G. Megariotis, S.G. Grdadolnik, M. Papadopoulos, D. Vlahakos, M. Maragoudakis, G. Liapakis, T. Mavromoustakos, J. Matsoukas, Rational design, efficient syntheses and biological evaluation of N,N'-symmetrically bis-substituted butylimidazole analogs as a new class of potent Angiotensin II receptor blockers, Eur. J. Med. Chem. 62 (2013) 352–370.

[8] I.V. Tetko, P. Bruneau, Application of ALOGPS to predict 1-octanol/water distribution coefficients, logP, and logD, of AstraZeneca in-house database, J. Pharm. Sci. 93 (2004) 3103–3110.

[9] T.R. Oliveira, M.T. Lamy, U.M. De Paula, L.L. Guimarães, M.S. Toledo, H.K. Takahashi, A.H. Straus, C.J. Lindsey, T.B. Paiva, Structural properties of lipid reconstructs and lipid composition of normotensive and hypertensive rat vascular smooth muscle cell membranes, Braz. J. Med. Biol. Res. 42 (2009) 844–853.

[10] M. Lucio, J.L.F.C. Lima, S. Reis, Drug-membrane interactions: significance for medicinal chemistry, Curr. Med. Chem. 17 (2010) 1795–1809.

[11] A.M. Seddon, D. Casey, R.V. Law, A. Gee, R.H. Templer, O. Ces, Drug interactions with lipid membranes, Chem. Soc. Rev. 38 (2009) 2509–2519.

[12] A. Ramamoorthy, Beyond NMR spectra of antimicrobial peptides: dynamical images at atomic resolution and functional insights, Solid State Nucl. Magn. Reson. 35 (2009) 201–207.

[13] H. Jerebek, G. Pabst, M. Rappolt, T. Stockner, Membrane-mediated effect on ion channels induced by the anesthetic drug ketamine, J. Am. Chem. Soc. 132 (2010) 7990–7997.

[14] R.S. Cantor, Lipid composition and the lateral pressure profile in bilayers, Biophys. J. 76 (1999) 2625–2639.

[15] C. Xing, O.H.S. Ollila, I. Vattulainen, R. Faller, Asymmetric nature of lateral pressure profiles in supported lipid membranes and its implications for membrane protein functions, Soft Matter 5 (2009) 3258–3261.

[16] C. Fotakis, G. Megariotis, D. Christodouleas, E. Kritsi, M. Zervou, P. Zoumpoulakis, D. Ntountaniotis, C. Potamitis, A. Hodzic, G. Pabst, M. Rappolt, G. Mali, J. Baldus, C. Glaubitz, M.G. Papadopoulos, A. Afantitis, G. Melagraki, T. Mavromoustakos, Comparative study of the AT1 receptor prodrug antagonist candesartan cilexetil with other sartans on the interactions with membrane bilayers, Biochim. Biophys. Acta 1818 (2012) 3107–3120.

[17] C. Fotakis, D. Christodouleas, P. Zoumpoulakis, E. Kritsi, N.P. Benetis, T. Mavromoustakos, H. Reis, A. Gili, M.G. Papadopoulos, M. Zervou, Comparative biophysical studies of sartan class drug molecules losartan and candesartan (CV-11974) with membrane bilayers, J. Phys. Chem. B 115 (2011) 6180–6192.

[18] C. Potamitis, P. Chatzigeorgiou, E. Siapi, K. Viras, T. Mavromoustakos, A. Hodzic, G. Pabst, F. Cacho-Nerin, P. Laggner, M. Rappolt, Interactions of the AT1 antagonist valsartan with dipalmitoyl–phosphatidylcholine bilayers, Biochim. Biophys. Acta 1808 (2011) 1753–1763.

[19] C. Fotakis, D. Christodouleas, P. Chatzigeorgiou, M. Zervou, N.-P. Benetis, K. Viras, T. Mavromoustakos, Development of a CP 31P NMR broadline simulation methodology for studying the interactions of antihypertensive AT1 antagonist losartan with phospholipid bilayers, Biophys. J. 96 (2009) 2227–2236.

[20] D. Ntountaniotis, G. Mali, S.G. Grdadolnik, M. Halabalaki, A.-L. Skaltsounis, C. Potamitis, E. Siapi, P. Chatzigeorgiou, M. Rappolt, T. Mavromoustakos, Thermal, dynamic and structural properties of drug AT1 antagonist olmesartan in lipid bilayers, Biochim. Biophys. Acta 1808 (2011) 2995–3006.

[21] T.M. Mavromoustakos, The use of differential scanning calorimetry to study drug-membrane interactions, Methods Mol. Biol. 400 (2007) 587–600.

[22] T. Mavromoustakos, P. Chatzigeorgiou, C. Koukoulitsa, S. Durdagi, Partial interdigitation of lipid bilayers, Int. J. Quantum Chem. 111 (2011) 1172–1183.

[23] U. Holzgrabe, I. Wawer, B. Diehl, NMR Spectroscopy in Pharmaceutical Analysis, Elsevier, Amsterdam, 2008.

[24] C. Fotakis, S. Gega, E. Siapi, C. Potamitis, K. Viras, P. Moutevelis-Minakakis, C.G. Kokotos, S. Durdagi, S. Golic Grdadolnik, B. Sartori, M. Rappolt, T. Mavromoustakos, Interactions at the bilayer interface and receptor site induced by the novel synthetic pyrrolidinone analog MMK3, Biochim. Biophys. Acta 1768 (2010) 422–432.

[25] I. Kyrikou, N.P. Benetis, P. Chatzigeorgiou, M. Zervou, K. Viras, C. Poulos, T. Mavromoustakos, Interactions of the dipeptide paralysin Ala–Tyr and the aminoacid Glu with phospholipid bilayers, Biochim. Biophys. Acta 1778 (2008) 113–124.

[26] I.W. Levin, R.N. Lewis, Fourier transform Raman spectroscopy of biological materials, Anal. Chem. 62 (1990) 1101A–1111A.

[27] R.K. Bista, R.F. Bruch, A.M. Covington, Variable-temperature Raman spectromicroscopy for a comprehensive analysis of the conformational order in PEGylated lipids, J. Raman Spectrosc. 40 (2008) 463–471.

[28] C.H. Huang, J.R. Lapides, I.W. Levin, Phase-transition behaviour of saturated, symmetric chain phospholipid bilayer dispersions determined by Raman spectroscopy: correlation between spectral and thermodynamic parameters, J. Am. Chem. Soc. 104 (1982) 5926–5930.

[29] D. Zhao, J. Feng, Q. Huo, N. Melosh, G.H. Fredrickson, B.F. Chmelka, G.D. Stucky, Triblock copolymer syntheses of mesoporous silica with periodic 50 to 300 angstrom pores, Science 279 (1998) 548–552.

[30] M. Vallet-Regí, F. Balas, D. Arcos, Mesoporous materials for drug delivery, Angew. Chem. Int. Ed. 46 (2007) 7548–7558.

[31] J.C. Doadrio, E.M.B. Sousa, I. Izquierdo-Barba, A.L. Doadrio, J. Perez-Pariente, M. Vallet-Regí, Functionalization of mesoporous materials with long alkyl chains as a strategy for controlling drug delivery pattern, J. Mater. Chem. 16 (2006) 462–466.

[32] A. Bernardos, E. Anzar, C. Coll, R. Martínez-Mañez, J.M. Barat, Ma.D. Marcos, F. Sancenón, A. Benito, J. Soto, Controlled release of vitamin B2 using mesoporous materials functionalized with amine-bearing gate-like scaffoldings, J. Control. Release 131 (2008) 181–189.

[33] Q. Yang, S. Wang, P. Fan, L. Wang, Y. Di, K. Lin, F.S. Xiao, pH-responsive carrier system based on carboxylic acid modified mesoporous silica and polyelectrolite for drug delivery, Chem. Mater. 17 (2005) 5999–6003.

[34] S. Giri, B.G. Trewyn, M.P. Stellmaker, V.S.Y. Lin, Stimuli-responsive controlled release delivery system based on mesoporous silica nanorods capped with magnetic nanoparticles, Angew. Chem. Int. Ed. 44 (2005) 5038–5044.

[35] A. Sayari, B.-H. Han, Y. Yang, Simple synthesis route to monodispersed SBA-15 silica rods, J. Am. Chem. Soc. 126 (2004) 14348–14349.

[36] T. Ukmar, A. Godec, O. Planinšek, V. Kaučič, G. Mali, M. Gaberšcek, The phase (trans)formation and physical state of a model drug in mesoscopic confinement, Phys. Chem. Chem. Phys. 13 (2011) 16046–16054.

[37] T. Ukmar, T. Čendak, M. Mazaj, V. Kaučič, G. Mali, Structural and dynamical properties of indomethacin molecules embedded within the mesopores of SBA-15: a solid-state NMR view, J. Phys. Chem. C 116 (2012) 2662–2671.

[38] X. Tian, S. Pavlopoulos, Y. De-Ping, A. Makriyannis, The interaction of cannabinoid receptor agonists, CP55940 and WIN55212-2 with membranes using solid state $^2$H NMR, Biochim. Biophys. Acta 1808 (2011) 2095–2101.